Smart Sensing Applications in Agriculture and Food Industry

Pilar Barreiro, Eva. Cristina Correa, F. Javier Arranz, Belén Diezma, Luis Ruiz, Morris Villarroel, J. Ignacio Robla, F. Javier García-Hierro

CONTENTS

INTRODUCTION

This chapter is structured in three main sections: an introduction to the smart concept and smart quality control, a review of the state of the art in integrated sensors, embedded systems, and the third one which is dedicated to a review of three case studies. The case studies refer to three results lines that are under taken by the LPF-TAGRALIA in the field of smart sensing. It provides examples of how to develop smart capabilities within standard low cost sensors. A variety of smart capabilities have been selected such as dynamic analysis of physical magnitudes, transmission diagnosis and such reliability and a full range of examples of analytical models of wood drying that can be incorporated to sensor chips to enhance sensor performs and to enable the term smart sensor.

Each of the three sections of the chapter is independent and so the reader can decide where to start from according to their particular expertise. For unfamiliar readers with smart technologies, all of them might be of interest, while for experienced readers in the subject the case studies directly are probably the most relevant issue.

WHAT IS IT TO BE SMART

Essentially, a smart product is such one that is able to interact with human beings, and that adapts to the context of the user without forcing him/her to adapt to it (Van Wylick, 2009). According to Serge Rijsdijk, as quoted by the previous author, a more complex definition of smart products includes one or more of following seven **dimensions**:

- **Ability to co-operate** with other devices.
- **Adaptability** to learn and improve the match between its functioning and its environment, i.e. my example of auto-changing gears or a thermostat that collects data about room and outer temperature and uses that to fulfill its user's wishes.
- **Autonomy,** meaning that the device can operate without interference from the user, e.g. some of those autonomous lawnmowers and vacuum-cleaners we keep hearing about.
- **Human-like interaction** that is interacting with humans in a fashion that feels natural to them.
- **Multi-functionality:** i.e. a single product fulfilling multiple functions, such as a modern mobile phone.
- **Personality:** meaning the product's ability to show the properties of credible personality, that is being proactive.
- **Reactivity:** i.e. the ability of a device to react to its environment in a "stimulus / response manner."

SMART QUALITY CONTROL: FROM SENSING TO ACTING

In this paragraph a summary of the National Project Smart-QC is provided, where four research groups[1] (LPF_TAGRALIA, LTS_CENIM, GSC, GIB_IIM) and two institutions (UPM and CSIC) interact within the same goal: smart quality sensing and control for the Agro-food industry.

As start point, the project states that Industry and particularly Food Industry, is nowadays facing critical changes in response to consumer needs, which in addition to health and safety awareness, demand an ever larger diversity of food products with high quality standards. Such variety in the demand, from the consumer side, is driven by social or ethical reasons as it is the case of products more compliant with the environment or produced by sustainable processes. On the other hand, food industry is in a permanent quest for new markets and new population sectors not accessible before, which immediately translates into the search for novel products and more efficient processes so to gain market opportunities with respect to other companies (Jurianse, 1999; Bruin and Jongen, 2003).

In order to satisfy such needs and demands, which although driven by the product, directly affect the process, novel and efficient food and process engineering approaches must be developed so to comply with the proposed requirements (Datta, 1998). Product engineering approaches are already responding to the challenge by proposing new methods and tools to systematically modify or even design new products in response to consumer needs (Aguilera, 2000; 2004). In similar terms, Process Engineering should offer efficient and flexible process alternatives to comply with the product safety and quality standards, while contributing to a sustainable production by minimizing operation costs and environmental impact.

However, and from the automation and control point of view, there are a number of limitations in food processing plants which could prevent an appropriate response to such needs (Sasha et al, 2001). Among those weakness and limitations, also detected in other process industries (Qin and Badgwell, 2003) one should highlight the following ones:

- Most plant control schemes reduce to local and **decentralized control loops acting on a usually very small number of states** (typically temperature or pressure) not directly connected with product quality and in many cases neither with critical aspects of the operation such as water or energy consumption.
- Although presently, many food plants benefit from advances in data acquisition and monitoring of the full production lines to gather and store huge amounts of data, **the use of such information is quite limited**, usually not efficiently employed and reduced to configure alarms (often handled at a very low level) or to help producing simple production decision rules and off-line control of inventories.

[1] LPF_TAGRALIA: laboratorio de propiedades físicas y tecnologías avanzadas en agroalimentanción.
LTS_CENIM: laboratorio de tecnología y sensores el Centro Nacional de Investigaciones Metalúrgicas.
GSC: grupo de sistemas complejos.
GIB_IIM: Grupo de Ingeniería de Bio-procesos del Instituto de Investigaciones Marinas del Consejo Superior de Investigaciones Científicas.

- Often recognized as a specificity of food processes, **the lack of sensors for relevant product characteristics is still a problem**. *Improving the reliability of sensing devices and developing new hardware-software sensing techniques to online estimate difficult-to-measure quality product parameters are critical in developing smart control applications for food factories.*

However, research is still needed to connect novel sensing techniques with advances in efficient modelling and simulation of quality kinetics and transfer models (essentially by defining accurate yet fast to integrate models) **so to build up smart sensors able to inline predict food quality attributes**.

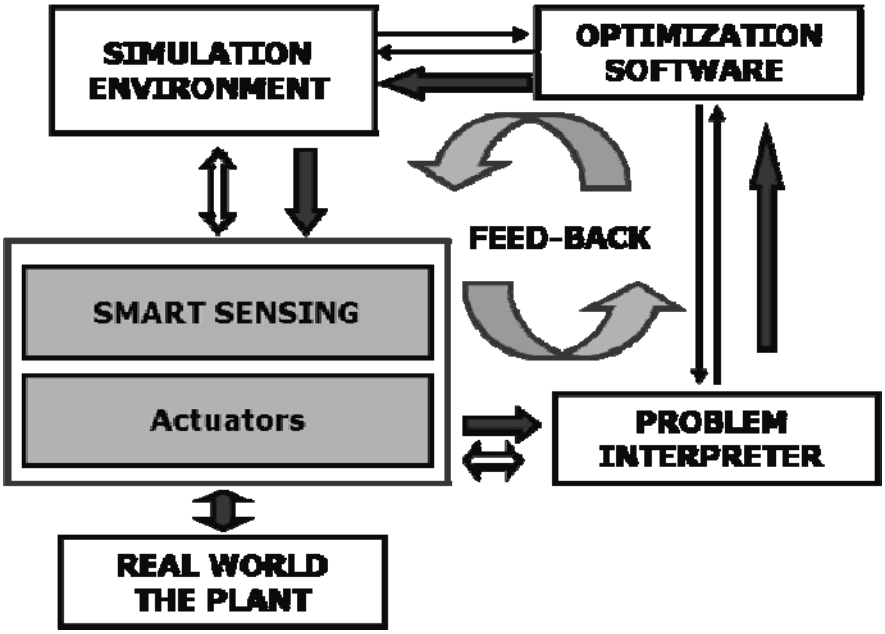

Figure 1. Smart-QC: The integral approach to optimal on-line control of food product quality through smart sensing techniques.

STATE OF THE ART

In this section, a general approach to smart sensor and controls is provided. The aim is to facilitate the understanding to unfamiliar readers with the subject. This section ends with some considerations on how to extend those areas towards higher level ones such as smart environments and machines, which might be interesting topics for experts within the Agricultural Engineering domain. Some specific applications that make profit of available embedded sensor and control technology will be afterwards described in the case studies

SMART SENSORS

According to Corsi (Corsi, 2007), the term **smart sensor** refers to those elements containing sensing and signal processing capabilities and understanding, with objectives ranging from simple viewing to sophisticated remote sensing, surveillance, search/track, robotics, perceptronics and intelligence applications (Corsi, 2007). The smart sensor is expected to have the capability that functionality and architecture, as well as raw data acquisition are based the existence of microprocessing unit (Son et al., 2009).

Rapid advances in sensors, wireless communications, Micro Electro Mechanical Systems (MEMS) have the potential to assist in dealing with a large amount of data that is generated by a monitoring system. On board processing at the sensor allows a portion of the computation to be done locally on the sensors' embedded microprocessor, with self diagnosis and self-calibration capabilities, thus reducing that data amount of information that needs to be transmitted over the network. It is important to state that the basic difference between a smart sensor and a standard integrated sensor is its intelligence capabilities (Spencer et al., 2004). Son in 2009 proposes the use of intelligent classification systems to assist the condition monitoring tasks by correctly interpreting the fault data in machine fault diagnosis. Result by these authors demonstrated the advantage of smart sensor systems compared to conventional ones.

Smart sensors move some of the reasoning work down to the physical level without the intention of solving the entire intelligent environment design problem, but to provide intelligent functionalities within the confines of a single object and task.

In order to get a better understanding of the development of smart sensors a deeper view into transducers and integrated sensors, as well as on MEMS is worth the trouble.

Transducers and Integrated sensors

In the last decade, the automotive market has become one of the main driving forces in the transducer field, since it requires highly reliable devices at very low price, and mass-produced

silicon sensors satisfy these requirements. According to Middlehoek (2000), the transducer field is moving in two opposite directions: the development of increasing complex and expensive processes in various materials to realize transducers with special characteristics, versus the use of standard processing steps to produce transducers with modest characteristics that can be greatly improved by designing the so-called smart sensors by ensuring that the sensor, the electronic circuitry, and the microcontrollers for the signal processing, are combined on one chip.

The transformation of non electrical quantities into electrical ones has to take into account that the physical or chemical magnitude is composed by a main and a side effect: the avowed one and the interference respectively. The design process for sensors needs to take into account these side effects, sometimes called cross sensitivity. The non-ideal properties during signal processing leads to faulty measurements, and so steps have to be considered to compensate for some of the side effects even when using analog circuits. These steps include the use of filters, signal-differences of two identical sensors, or special circuits to suppress the null drift. When the non-linear characteristics of a sensor do not vary over time, it is possible to linearize or adjust them by using the microcomputer. This enables the calibration of each sensor during its manufacturing. The use of microcontrollers makes frequency modulated and incremental sensors economical because of built-in counters which are able to measure frequencies easily. Further improvement is possible by integration of sensor, signal processing, ADC[2] and micro-computer with bus interface into one single unit. This integration (possibly into one single chip) has several important advantages: reduction of the costs for large scale manufacturing, reduction of space requirements, higher precision, and decrease of susceptibility to noise. Because of this integration, however, the requirements for robustness and reliability increase because a sensor is often subject to a rough environment. The fact that all of algorithms may be programmed individually for each sensor is very important, and further possibilities arise with the use of multi-sensor technology, i.e. combination of similar or different types of sensors, and with the many developments now emerging through micromechanics (Isermann, 2006)

The most important criteria for evaluating sensors are the static behavior, dynamic response, quality class and measuring range, overload capacity, compatibility with associated components, environmental influences, and reliability application for consumer goods do not need a high accuracy (2% to 5% are sufficient). Industrial application, on the other hand, require much higher precision (0.05% to 1), with typical overload capacity between 200% and 500% (Isermann, 2006). The reliability of a sensor is described by characteristic parameters such as the mean time to failure (MTTF, h) or its reciprocal value, the mean failure rate (h^{-1}).

Micro Electro-Mechanical Systems (MEMS) and Smart Dust

A very interesting view of MEMS evolution is provided by Wise in 2007 (**Figure 2**), who states that since the early days of microelectronics (1950) there was a strong interest in using silicon

[2] ADC: Analog to Digital Converter, conversor anlógico-digital.

technology to transduce mechanical, chemical, optical, and thermal events into electronic signals themselves.

According to the same author (Wise, 2007), the term micromachining included in 1960: diaphragms, cantilevers[3], valves, heaters, fluidic channels, and other structures developed in silicon, while by the end of 1980 the United States Science Foundation started to fund this area at a substantial level area, which was becoming known as MEMS. The last decade of past siècle saw the proliferation of many different sub-disciplines such as: bio-MEMS, RF-MEMS, optical-MEMS, inertial-MEMS and microfluidics (**Figure 3**), while from the start of this century there is an increasing convergence of sensing with embedded computing and wireless technology.

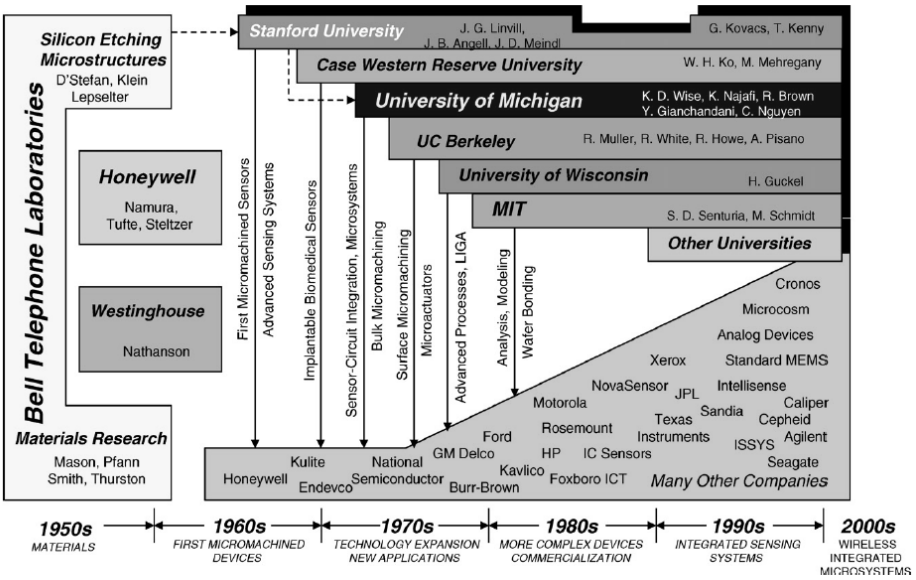

Figure 2. Evolution of integrated sensors, MEMS, and Microsystems in USA, (Wise, 2007).

The term Smart Dust has come to be used to describe a wide range of wireless sensor network hardware at a small scale down to a handful of cubic millimeters, where each wireless sensor node or mote contains one or more sensors, hardware for computation and communication and power supply. Motes are assumed to be autonomous, programmable, and able to participate in multihop mesh communication (Cook et al., 2006).

According to the same author, the genesis of Smart Dust can be dated in 1992. The first wireless sensor motes, called COTS[4] Dust, were built early in the Smart Dust Project using printed circuit boards and off-the-shelf components. COTS and other macro-scale motes

[3] Cantilever: a beam supported on only one end. Cantilevered beams are the most ubiquitous structures in the field of microelectromechanical systems (MEMS, commonly fabricated from silicon (Si), silicon nitride (SiN), or polymers.

[4] COTS: Commercial of the Shelf

(**Figure 4**) were developed to explore sensor network software and individual mote architecture, as well as to deploy small scale networks. The Mica mote is the most popular mote used in research (see case study 2), and was developed to mimic expected architecture of a highly integrated mote while using off-the-shelf parts mounted on common PC board to reduce development time.

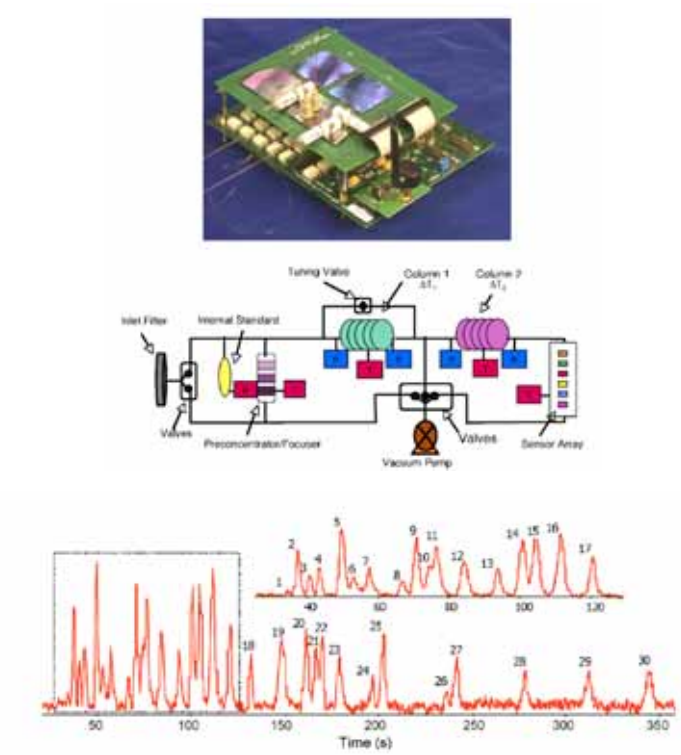

Figure 3. Integrated Chromatography System; this system displaces 200 $cm^3$and detects 30 air pollutants are detected using a single 3m-long-silicon-glass column. The separation channel is 150 µm wide and 240 µm deep, chip size is 1.2cm x 1.2 cm (Wise, 2007).

The smallest mote to date displaces only 4 mm^3 and contains a 8-bit ADC[5], an optical receiver, a light sensor, an accelerometer, a multi-voltage solar cell power source, and limited computation (**Figure 5**). Even these highly integrated chips require an off-chip battery, some passive components, a crystal timing element, and a RF antenna, resulting in a complete package at the centimeter to inch scale. Besides, a main concern with Smart Dust is the need to locate the motes when ubiquitous measurements are performed, and so there is a demand to discover built-in location capabilities into the network. As the cost of mote falls and the number of wireless sensors increases, the cost of locating installed sensors will drive the development of automatic location discovery, which is critical for tracking and tracing applications, as well as environmental monitoring. Furthermore, many applications will require mobile motes with the ability of dynamically update position information (Cook et al., 2006).

[5] ADC: Analog to Digital Converter

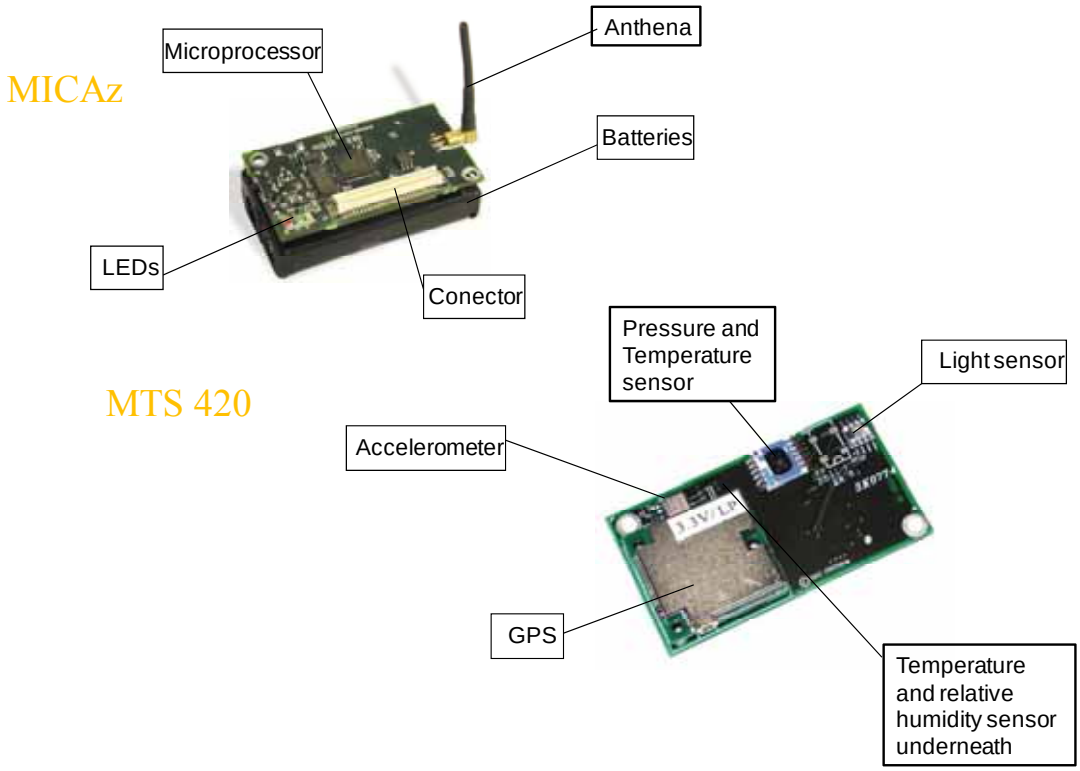

Figure 4. The Crossbow motes (MICAz or Xbow), well know commercially available Zigbee motes with sensor card (MTS 420).

The same authors indicate that the average power consumption of an inch-scale mote must be in the range of tens to hundreds of microwatts or just a few joules per day for battery lasting from one to over 10 years. Such a feature will require deep duty cycling, that is to say, the hardware should be able to quickly transit between powered and unpowered state. Moreover, turning the RF off 99% of the time is easy, but knowing when to turn it on again is not. Both electrostatic MEMS devices and PZT[6] transducers can be used to harvest energy from the ambient mechanical vibrations or sunlight. Thin film batteries seem to be promising for storing the energy harvested. It is expected that the described system-in-chip will be commercialized in not far time travel, providing secure wireless communication at hundreds of kilobits per second over tens of meters, offering multihop networking, onboard sensors, 10 to 16-bit ADC and sensor datapath.

[6] PZT: Piezoelectric

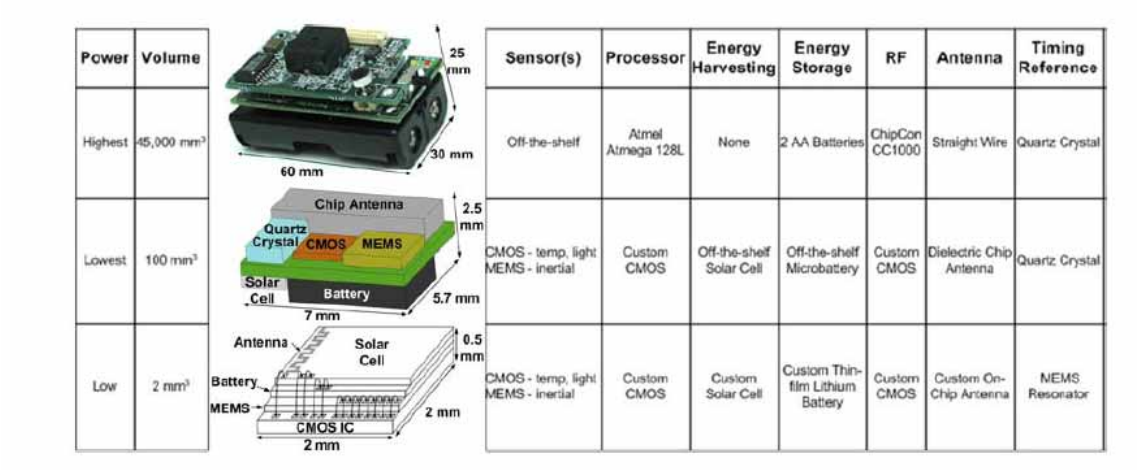

Figure 5. A complete sensor node may be implemented with varying levels of integration (Cook et al. 2006).

SMART CONTROL

In this paragraph, it is intended to include the vision of smart control in the context of the Project Smart-QC, which covers a description of methods and tools for: modeling and simulation, model identification and validation, real-time optimization and control, and the vision for embedded integration. This task is mainly addressed to GIB:IIM and GSC, but needs a constant feed back of the rest of the groups in terms of description of quality, model definition and smart sensor response.

Modelling and simulation

When considering food quality modelling, there is a need to face the spatial distribution (**Figure 6**) and thus the underlying mass, energy and momentum balances needed to provide a detailed evolution of product quality and safety in refrigeration and thermal processes, and the wide range and complexity of the possible spatial geometries (domains), detailed models need to consider the finite element method (FEM), complemented when needed with CFD[7] codes describing momentum balances.

First principle modelling and model reduction through projection techniques can be used so to reduce the dimensionality of the original sets of partial differential equations (Balsa et al, 2002a; 2002b). The underlying techniques are applied to derive methods for optimal sensor (and actuator) location (Alonso et al, 2004) and more recently to reconstruct the time and spatial distribution of variables such as temperature or fluid velocity fields from partial measurements (Garcia et al, 2007).

[7] CFD: Computational Fluid Dynamics

The FEM formulation facilitates the model reduction processes either through LSD (Laplacian Spectral decomposition) or PODs (Proper Orthogonal Decomposition) as demonstrated in the work by Alonso et al, 2004, and Garcia et al, 2007. Both techniques can be applied and compared in the present research work as tools to construct operational models for smart quality sensors and on-line quality optimal control

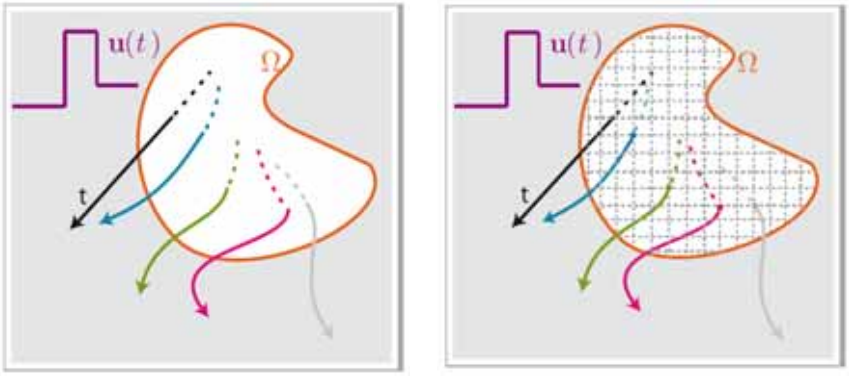

Figure 6. Model formulation: either in temporal (left) or spatial-temporal domain (right).

Quality attributes in refrigeration or in thermal processes (usually related with nonlinear chemical or microbiological kinetics) completes the systems description by incorporating such terms as production into the first principle models. For the thermal processes considered, the kinetics describe the effect of process conditions (specially the effect of temperature-time profiles) on safety and quality parameters such as lethality in the first case, or color, texture, moisture or vitamin content as example of the second type of parameters (Balsa-Canto, 2007 and references there in).

Basic physiological processes underlying perishable products in refrigeration are generally well understood and have been used by LPF_TAGRALIA (see **Figure 7** and **Figure 8**)for modelling examples of dynamic behavior of apples under storage (De Smedt et al., 2002). The modelling procedure includes sensitivity analysis to address the variance covariance matrix for all the parameters estimated in a model and thus the robustness of data extracted with them.

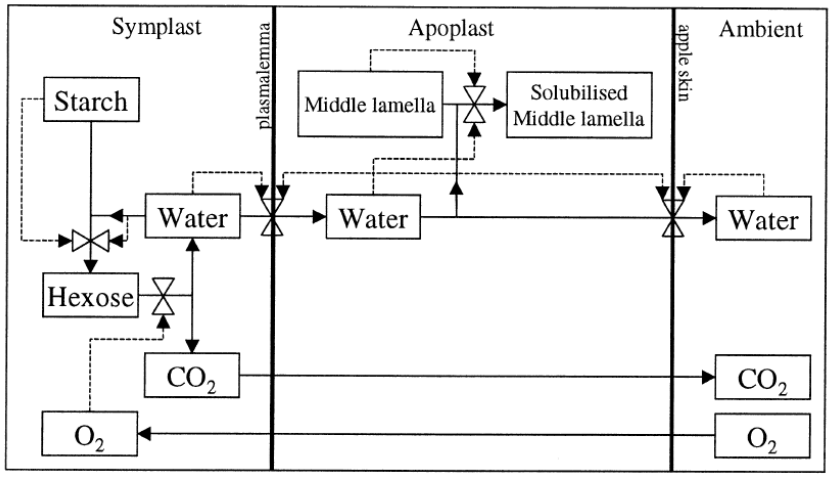

Figure 7. Basic processes underlying perishable products in refrigeration (De Smedt et al., 2002).

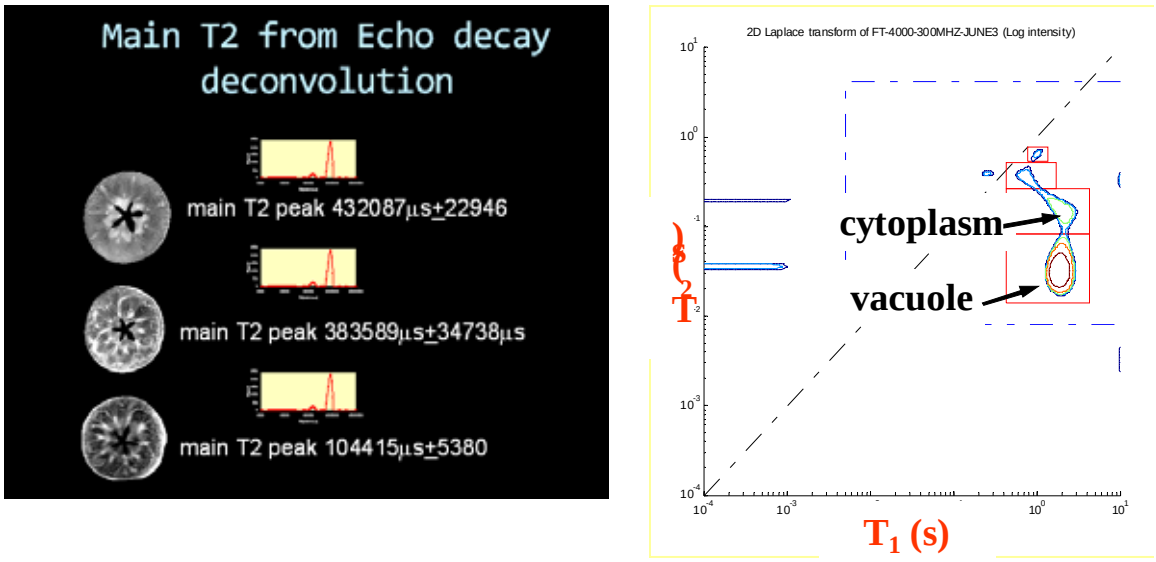

Figure 8. MRI and NMR relaxometry as example of techniques that LPF_TAGRALIA has used to address spatial-temporal changes of quality in fruits.

Embedded CONTROL SYSTEMS

Models and real-time optimization methods could be in time embedded into a micro-computer by means of dedicated software development using very high-level languages (fourth generation languages, 4GL) such as Matlab or its free source equivalent R (for statistical purposes) and OCTAVE (for numerical computation), or direct programming in FORTRAM (third generation language, 3GL).

The goal of such 3GL and 4GL is to make programming accessible to non-specialized programmers, some of which are used for rapid prototyping and rapid application development. Many of such 4GL are based on pre-written components which may be functions in the traditional approach, or object oriented in the more recent one (Saraiva et al, 2006).

SMART ENVIRONMENT

We can expand the view of the smart concept to smart environment, which has been defined by Cook (Cook et al., 2007) as one that is able to acquire and apply knowledge about the environment and its inhabitants in order to improve the experience in that environment. Automation in a smart environment can be viewed as a cycle of perceiving the state of the environment, reasoning about the state together with task goals and outcome of possible actions, and acting upon the environment to change the state. Among the desired features in a

smart environment, sensor/actuator networks need to be fast, easy to install and maintained, robust and self organizing to create a ubiquitous/pervasive computing platform.

Most of the concepts proposed for smart sensors and controls can be used in this context, however the term smart environment stresses the need of interaction between the components with some kind of global intelligence that will enable to predict the inhabitants (people, animal or plants) needs and preferences.

In agriculture controlled environments such as greenhouses, food and fruit storage and transport, or animal livestock buildings are direct potential users of such technology.

SMART MACHINES

Another potential user of smart sensors and controls falls within the domain of designing Smart Machines which stresses the creation of simple, stand-alone systems that use embedded processors. Within this goal, it is important to remain current in new sensors, actuators and interfacing methods which are being introduced at a rapid pace with a trend towards lower cost and higher performance. The appropriate integration of mechanics, electronics and information is critical to the success of many current products and experimental systems (Durfee, 1995). Tomizuka in 2002 summarizes the process of evolution of mechatronics towards smart machines (**Figure 9**).

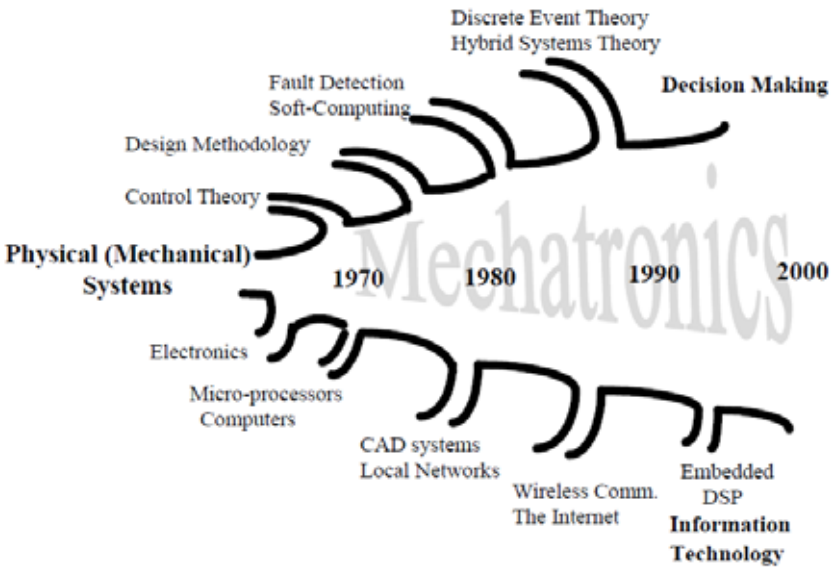

Figure 9. Evolution of Mechatronics (Tomizuka, 2002)

Barbara et al. (2004) propose a task analysis and decomposition procedure to derive and organize the knowledge for the control of smart machines such as autonomous vehicles. The

procedure summarized by Master students of LPF_TAGRALIA (**¡Error! No se encuentra el origen de la referencia.**), covers six different steps: task decomposition design, agent[8] module organization, state table definition, situation dependencies on world behavior, world state dependencies, and measurement resolution. This paper points the need of facing an integrated view of system characteristics, system components, behavior and tasks

Collaboration among smart machines is another hot topic that is expected to expand in the forthcoming years. Arguenon et al. (2006) propose a multi-agent based prototyping for grape harvesting using small teams of smart collaborating robots.

[8] Agent: A piece of software that acts for a user or other program in a relationship of agency.The idea is that agents are not strictly invoked for a task, but activate themselves.

CASE STUDIES

Three case studies have been selected that represent a variety of Ag-Engineering applications. We shall start by presenting the simplest approach to date towards a smart sensor, which is based on the analysis of phase space changes concerning temperature and air enthalpy along trans-border pig transport. In the second case, we propose several ways to face either smart capabilities for sensor fault diagnosis (communication errors and measurements reliability), or either system diagnosis, i.e. billing errors in energy consumption that occur due to valves miss function. Finally, several approaches are proposed as to assess wood drying by means of simple temperature and humidity sensors and several considerations on mass and energy balances.

SMART CONCEPT FOR ANIMAL WELFARE

The hypothesis in this work is that environmental temperature and relative humidity affect animal production though little has been described about the effect of relative changes in enthalpy on pig welfare. Presumably, at the farm level where animals spend most of their lives, temporal changes in temperature and relative humidity are moderate. However, during live transport, environmental conditions can change abruptly, with unknown implications for animal welfare. The complete work (Villarroel et al. 2010) has been submitted to Biosystems Engineering and is currently under evaluation.

The environment: international animal journey. Seven journeys were made from Scotland to Malaga (Spain) between the months of May and October in 2008, with a commercial livestock transport vehicle carrying 80 pigs on each trip. The loading and unloading dates and average temperatures and humidity were all noted, as well as the average temperatures inside and outside the vehicle during transport (Table 1). Pigs were loaded in Edinburgh, taken via a ferry crossing of the English Channel to Fougeres in France, where they were unloaded from the vehicle and rested for the mandatory 24 hour period. After that rest period, the pigs were reloaded and taken to an abattoir in Humilladero, Malaga (Spain). All pigs were Landrace x Large white, and approximately 100 kg live weight.

Sensors on farm, during transport and at abattoir: consisting at this stage of Data loggers (Onset computers, Hobo H8 loggers) to measure temperature and relatively humidity around the pigs before loading, during transport and at the abattoir. Two sensors were placed on the farm in two pens near the experimental animals and recorded once every 30 min from May to October. Two more sensors were placed inside the lairage pens and also recorded once every 30 min from May to October.

Prior to loading the vehicle, data loggers were mounted on the partition gates between the pens on the middle deck. The data loggers were protected from direct contact and damage by the pigs by housing them in a perforated steel framework and were pre-programmed to

record, at regular 2 min intervals. Sensors on the truck were fitted and removed before and after each journey.

The measurements of air temperature and relative humidity were continuous throughout the whole transport period from Ellenthorpe to Humilladero. When the pigs were unloaded at Fougeres, though the data loggers remained on the vehicle, the conditions experienced by the pigs were very similar to those on the empty truck because of the open nature of the housing pens at the control post. In addition, there was good agreement between the conditions on the vehicle and those recorded by the ambient loggers.

Proposed models:

Psychrometric model. The psychrometric charts produced using the data collected from the sensors were computed based on the ASABE model which includes temperature, relative humidity, absolute humidity and enthalpy. The psychrometric data ASAE D271.2, defined in April 1979 and reviewed in 2005 (ASABE 2006 St. Joseph, MI) were used to calculate the psychrometric properties of the air at farm, during transport (both outside and inside the vehicle) and at the abattoir. Further explanation of this model is provided later-on in the text.

Phase space computation with Savitzky-Golay algorithm that addresses the temperature derivative with one-dimensional smoothing, and calculates the numerical derivatives. A polynomial is used to fit the data surrounding each data point. The smoothed points are computed by replacing each data point with the value of its fitted polynomial. Numerical derivatives arose after computing the derivative of each fitted polynomial at each data point. In our case a window of 21 points was used with a five order polynomial. A plot of temperature versus temperature derivative and enthalpy versus enthalpy change are used as phase spaces at each sensor location. It is then possible to compute the area of the different polygons that include all the data points in the phase space per journey (P_{area}).

Application: All seven journeys were completed with no injuries to the pigs or mortalities, between June and October 2008. The average journey length, including the rest period at Fougeres, was 63.3 hours. In journeys 6 and 7, slightly less than 80 pigs were loaded since 3 and 1 pigs, respectively, were deemed unfit for transport (pre-loading). Average temperatures were highest during journeys 3 and 5, while average relative humidity was highest in journey 4 (Table 1).

Table 1. Summary of the number of minutes that pigs were exposed to temperatures above 30ºC (>30ºC) and above 35ºC (>35ºC).

Trip	1	2	3	4	5	6	7
>30ºC	0	0	203	338	297	66	0
>35ºC	0	0	50	1	0	0	0

Since temperature and humidity values were taken every 2 minutes during transport, we obtained a total of 1900 data points (over 63.3 hours). The changes in temperature during transport are shown in **Figure 10** (right) for journey 3, under some of the hottest conditions.

According to the psychrometric charts obtained, the enthalpy of the air surrounding the pigs at the farm in Scotland, during transport and at the abattoir in Spain largely overlapped (**Figure 10**, left). Although temperatures were slightly lower in Edinburgh and higher in Malaga, the average enthalpy values ranged between 0.005 and 0.02 kg water/kg dry air.

However, the gradient of change in temperature was much higher during transport than at the loading or unloading sites (data not shown). The change in ambient temperature during transport varied between -0.025 and 0.025 ºC/s during transport, 10 times higher than the range of changes at the farm (0.008 and -0.001 ºC/s) or abattoir, (0.008 to -0.008 ºC/s).

Similarly, the gradient in change of enthalpy (**Figure 10**, right) was much higher during transport, (0.08 to -0.08 kJ/kg dry air per second), than at loading (0.002 to -0.002 kJ/kg dry air per second), or unloading (0.0025 to -0.0015 kJ/kg dry air per second).

Calculating the gradient of change in temperature or enthalpy produces different polygons per sensor, for which we calculated their areas (**Table 2**) in the case of temperature phase space. The area was smallest for trip 1, and highest for trip 3, which corresponds with the range of temperatures for those trips, but also with the speed of change in temperature.

With regards to current legislation, we also calculated the number of minutes that pigs were exposed to temperatures above 30ºC or 35ºC. Temperatures were above 30ºC on four journeys (3, 4, 5 and 6) but only above 35ºC for more than one minute on trip 4.

Main Achievements: In this studied we noted temperature and humidity values at the farm, during transport and at an abattoir, and calculated the temperature and enthalpy derivatives, which were highly correlated with a behavioural assessment of animal welfare post-transport. Our results suggest that the gradients in temperature and enthalpy during transport provide a sensitive non-invasive indicator of animal welfare. According to the psychrometric charts, air enthalpy did not vary widely at the loading or unloading sites or even during transport, indicating that temperature or relative humidity alone do not indicate environmental stress.

Although there are well established guidelines regarding enthalpy values and appropriate ranges in pig production (Whittemore & Kyriazakis, 2006), less information is available on changes in enthalpy with time (enthalpy gradient), probably since relative changes are quite low in normal farm environments. During transport, however, we have found that both temperature and enthalpy gradients vary much more quickly. Our exhaustive analysis of temperature and relative humidity on seven journeys (13300 data points in total), suggests that both temperature and enthalpy values increase or decrease at least 10 times faster during transport compared to the farm or abattoir, up to 1.5ºC min^{-1}, compared to 0.48ºC min^{-1} on the farm or abattoir. In addition, when more relative change was experienced by the pigs, they spent more time drinking after transport, indicating that those conditions are more stressful.

Concerning the development of smart sensors, it seems rather clear that a single sensor such as temperature does provide real-time information of the heat dynamics of the system, when using the phase space representation which goes far beyond the actual use of simple temperature threshold. Taking into account that temperature sensors are mandatory by EC regulations under animal transport, a real-time analysis may significantly contribute to improve animal welfare in trans-border travels.

Table 2. Summary of the areas of the polygons ($P_{area,}$) that included all the data points in the temperature phase space per journey. Each area is an average of the four sensors (N) on the vehicle (except for trip 7 which had 10 sensors). A low area implies a gradual change in temperature, even though the range in temperature may have been high. The %Max is area of that trip divided by the maximum area found among all sensors for all trips (a sensor in trip 3). SE is the standard error for area (SE_{area}) or maximum percentage ($SE_{\%max}$).

Trip	1	2	3	4	5	6	7
N	4	4	4	4	4	4	10
P_{area} ($ºC^2/s$)	0.071	0.102	0.389	0.12	0.151	0.133	0.101
SE_{area}	0.02	0.02	0.02	0.02	0.02	0.02	0.01
% Max	13.8	19.7	75.3	23.1	29.2	25.8	19.5
$SE_{\%max}$	4.7	4.7	4.7	4.7	4.7	4.7	2.9

Figure 10. Psychrometric charts on a) farm before loading in Scotland (Edinburgh), with the two different colours referring to two separate sensors, b) during transport inside the livestock vehicle from Scotland to Spain, where different colours are different journeys, and c) at the abattoir in Malaga (Humilladero, Spain), where the two colours are also two sensors. The relative phase space of enthalpy values during transport roughly overlaps with those normally experienced by the pigs on the farm.

a)

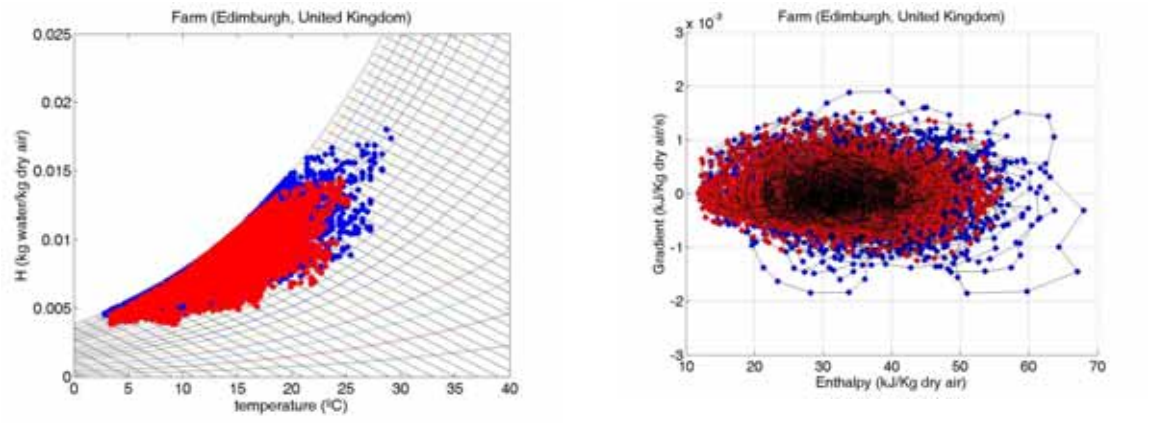

b)

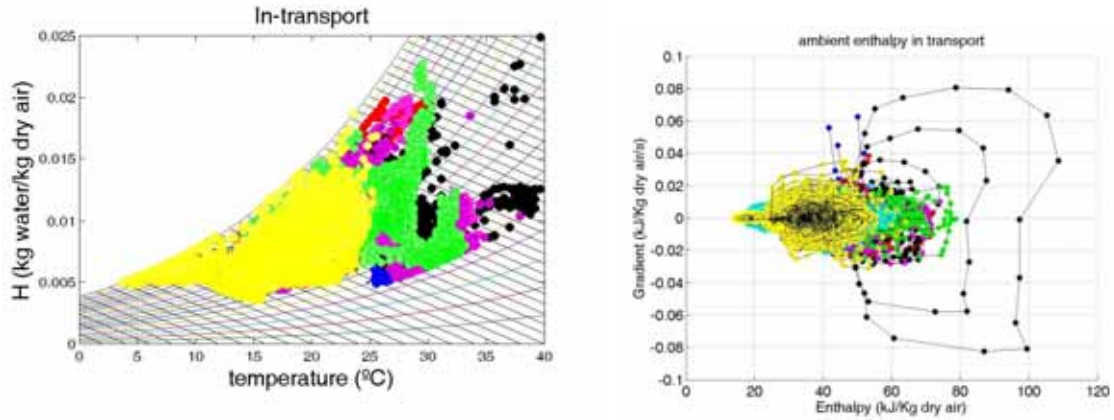

c)

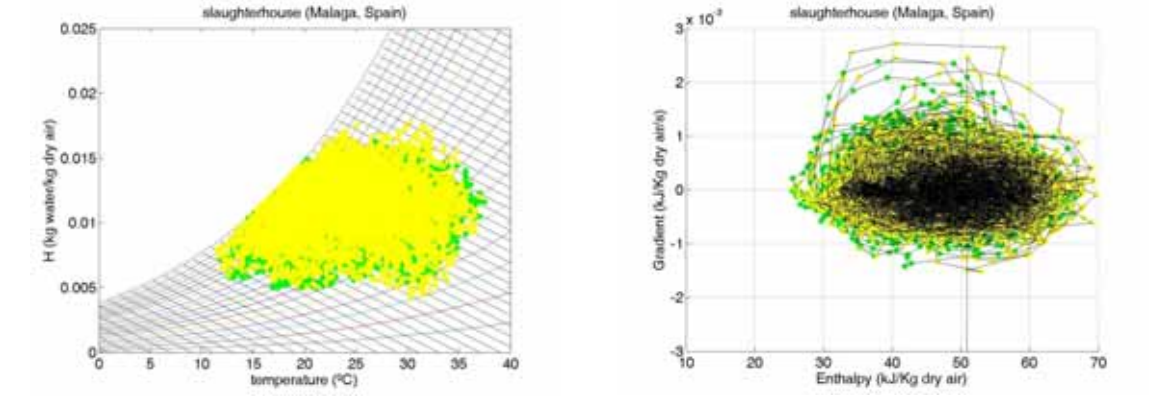

SMART SUPERVISION OF FOOD STORAGE AND TRANSPORT

The starting point for this case study indicates that the quality of fruits and vegetables changes rapidly when inadequate temperature and relative humidity conditions during transport and storage occur, being such inadequate temperature the second factor on the list causing foodborne illness, surpassed only by the initial microflora present in foods (Ruiz-García, 2007 and 2010; Rodríguez-Bermejo, 2007). Besides, fuel prices increase, climate change issues and rising air pollution has prompted governments, businesses and citizens to worry about energy saving. The refrigeration food preservation needs a good deal of energy input in places with hot weather. For example, the cold chambers studied in this work (1,700m^3 and 8 ºC Setpoint Temperature), consume energy of about 3,500Kcal/month in winter, and 7,500Kcal/month in summer. The work presented here covers the contents of the work published by Ruiz-García et al. in 2008, together with a congress communication to be presented at AgEng in September 2010 (García-Hierro et al., 2010).

The industrial environment: refrigerated chambers. Models were tested on data from three commercial wholesale refrigerated stores, numbered 11 (13 days), 29 (8days) and 40 (4 days). Each of which has a volume at of 1,716m^3, 26x6x11m, with an on/off glycol cooling system and insulated walls built of foam sandwiched between two layers of corrugated plate (total wall thickness is 0.16 m). The set points experimentation time were different for each one. Each chamber has a common pre-chamber space where a devoted sensor is placed. Therefore, three different ambient conditions occur: outdoor, pre-chamber and inside chamber with well known set point.

Sensors, Zigbee motes. Two ZigBee/IEEE 802.15.4 motes (transmitters) and one base station (receiver) were used, manufactured by Crossbow® (Ruiz-García, 2009 and 2010). One mote was installed outside the chamber, close to the door and the other one inside, at the other side of the wall. Sample rate was set to 180 s.

They have a microcontroller board (IRIS) together with an independent transducer board (MTS400) attached by means of a 52 pin connector. Its processor & radio platform is a XM2110CA, based on the Atmel ATmega1281. The RF power was configured to 3dBm (three times over previous MICAZ Motes). Power was supplied by two AA lithium batteries.

The MTS400 board hosts a variety of sensors: temperature and relative humidity (Sensirion SHT), barometric pressure and temperature (Intersema MS5534B), light intensity (TAOS TSL2550D) and a two-axis accelerometer (ADXL202JE). A laptop computer is used as the receiver, and communicates with the nodes through a Micaz mounted on the MIB520 ZigBee/USB gateway board; this device also provides a USB programming interface. In this study only the data from Sensirion and Intersema is used.

The Sensirion SHT is individually calibrated in a precision humidity chamber. The calibration coefficients are programmed into the memory. These coefficients are used internally during measurements to calibrate the signals from the sensors.

The MS5534B is a SMD-hybrid device including a piezoresistive pressure sensor and an ADC-Interface IC. It provides a 16 Bit data word from a pressure and temperature (-40 to +125°C) dependent voltage. Additionally the module contains 6 readable coefficients for a highly accurate software calibration of the sensor.

Up to six ZigBee/IEEE 802.15.4 motes (transmitters) and one base station (receiver) were used, manufactured by Nlaza®. One mote was installed outside the chamber, close to the door and the others inside in different positions, at the other side of the wall. Sample rate was set to 180s.

Its processor & radio platform is based on the Freescale MC13213. It's one of the second-generation ZigBee platform which incorporates a low power 2.4GHz radio frequency transceiver and an 8-bit microcontroller into a single 9·9·1mm 71-pin LGA package. Power was supplied by three AA lithium batteries that provide it a life time of several weeks.

A laptop computer is used as the receiver, and communicates with the nodes through RS-232 gateway /ZigBee ND-07 board. We can programme the nodes with Sensatel® software. The ND-11 board hosts an unique Sensirion SHT sensor.

Proposed models:

Fault diagnosis. Percentage of lost packages (*p*, %) in transmission is computed by identifying the multiple sending failures (*m*) and dividing by the number of theoretical packages (**Figure 11**). An *m* failure occurs whenever the elapsed time (*ET*, s) between consecutive packages follows the restriction: 1.5x*m*xSR<***ET***<1.5x*m*xSR, being SR the sampling period (s). The theoretical number of packages is then computed as total duration (s) divided by sampling period (s). The standard error (*SE*) associated to the ratio of lost packets is computed based on a binomial distribution as expressed in equation $SE = \sqrt{\frac{p(1-p)}{N}}$ Eq. 1, where *N* is the theoretical number of packages sent, and *p* is the ratio of lost packages.

$$SE = \sqrt{\frac{p(1-p)}{N}} \qquad \text{Eq. 1}$$

Besides data reliability is addressed by analyzing the first and second derivative of measurements, since it has been found that those values greatly increase when battery failure is to occur (**Figure 12**).

Psychrometric model. As mentioned in previous case study, the ASAE D271.2, defined in April 1979 and reviewed in 2006, is used for computing the psychrometric properties of air (ASABE, 2006).The Eq. 2 to Eq. 5, and **Table 3** enable the calculation of psychrometric data of air whenever two independent psychrometric properties of an air-water vapour mixture are known in addition to the atmospheric pressure.

$$Ps = e^{31.96 - \frac{6,270.36}{T} - 0.46 \cdot \ln T}$$

$$255.38\text{K} \leq \text{T} \leq 273.16\text{K}$$

Eq. 2

$$\frac{Ps}{R} = e^{\frac{A + B \cdot T + C \cdot T^2 + D \cdot T^3 + E \cdot T^4}{F \cdot T - G \cdot T^2}}$$

$$273.16\ \text{K} \leq \text{T} \leq 533.16\ \text{K}$$

Eq. 3

$$P_v = P_s \cdot \frac{RH}{100}$$

Eq. 4

$$H = \frac{0.6219 \cdot Pv}{Patm - Pv}$$

Eq. 5

where T is air temperature (K), P_s refers to the saturation vapor pressure (Pa), P_v to the vapour pressure (Pa), H to absolute air humidity (g/kg dry air), and P_{atm} to atmospheric pressure (Pa) (ASABE, 2006).

Table 3. Coefficients used to compute the psychrometric data (ASABE, 2006).

R=22,105,649.25	D=0.12558x10^{-3}
A=-27,405.526	E=-0.48502x10^{-7}
B=97.5413	F=4.34903
C=-0.146244	G=0.39381x10^{-2}

The Air Enthalpy and Power Consumption model. The air enthalpy inside and outside the cold store is computed by means of the psychrometric model (kcal) corresponding to ASAE D271.2), using the temperature and relative humidity obtained from the Crossbow motes and some considerations regarding the actual air movement inside the chamber. On the other hand the real power consumption of the chamber is provided hourly by the warehouse holder based on the temperature increase in the glycol system.

The cold chamber has got a defrosting system that reverses the glycol flow as to heat the evaporator and remove the water condensed on it accordingly; therefore defrosting periods are disregarded for energy billing. Whenever the valve that reverses the glycol flow fails to close, even though commanded, an overrated energy consumption assessment takes place. In such cases, the high temperature of the glycol flow is addressed to the need of cooling of the perishable product inside the store.

A proposal in this study is to check whether the energy billing does agree with the actual enthalpy increase in the air inside the chamber as a fault diagnosis procedure for the valves as well. Therefore, we set a new parameter for the analysis of possible errors in the billing of energy consumed: the subtraction of the energy consumed and the air enthalpy (*Diff)*. We

establish that there are billing errors and malfunctioning valves when a value for this parameter (*Diff*) is outside the limits of the statistically estimated range where it is the 95 or the 98 per cent of the values.

$$\text{Upper Limit(Kcal)} = \bar{x} + t \cdot s$$

$$\text{Lower Limit(Kcal)} = \bar{x} - t \cdot s$$

$$\bar{x} = \text{Diff mean}, \quad s = \text{Diff standard deviation}, \quad t = \text{t Student} = \begin{cases} 1.96 \text{ for } 95\% \\ 2.32 \text{ for } 98\% \end{cases}$$

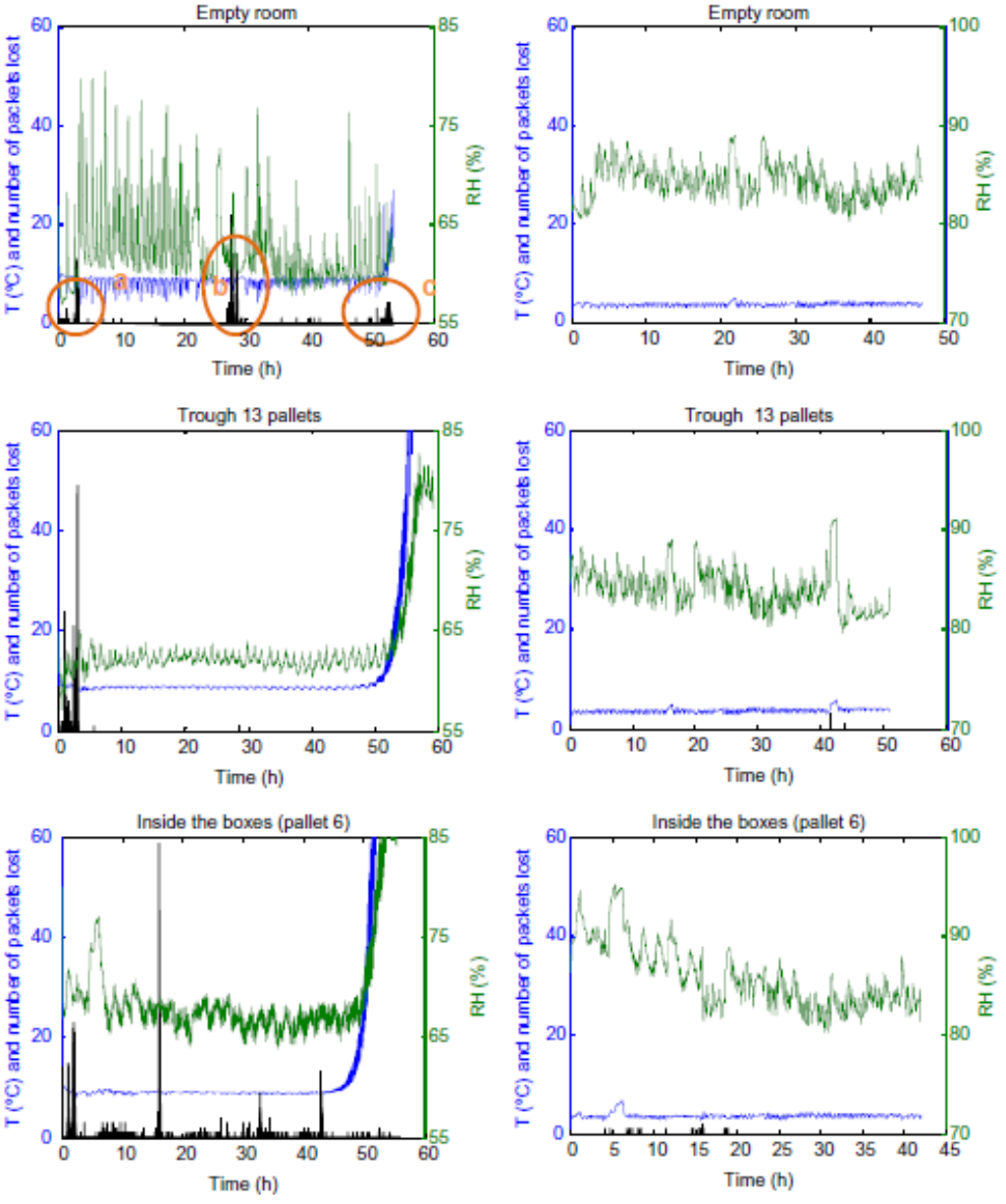

Figure 11. Relative Humidity (%), temperature (ºC), number of packets lost in two different types of Zigbee motes: Xbow (left), and Xbee (right); a, b and c stands for periods of accumulation of lost packages (Ruiz-García et al, 2008).

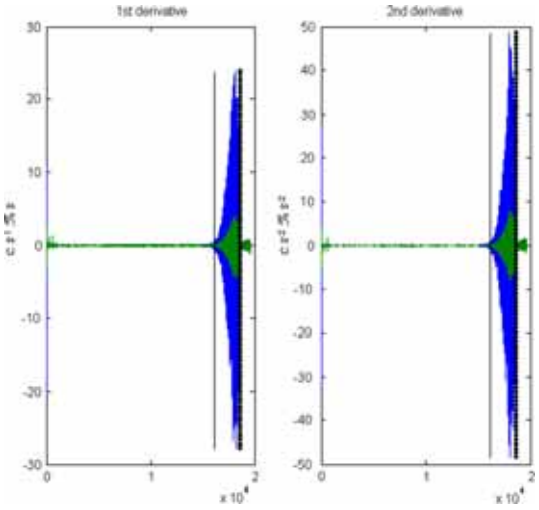

Figure 12. First and second derivative of Xbow temperature and relative humidity data, the wide increase in oscillation indicates that battery level is getting too low (Ruiz-García et al, 2008).

Application: Psychrometric charts for chambers number 40 is included in **Figure 13.** Psychrometric chart for cold chamber number 40 data., which illustrate the evolution of air absolute humidity (H, kg of water/ kg of dry air) related to the T (ºC). There are several clouds of data that corresponds to the Nlaza® motes placed in the sides that the figure indicates. Door openings created an increment in T (ºC) and H (kg of water/ kg of dry air), which then returns to normal again once the door is closed. The door of cold store number 40 keeps open longer, therefore cloud of data that corresponds to the mote placed outside the chamber is closer to clouds of motes inside the chamber data. When the door of the cold chamber is opened, warm air from the outside mixes with the air inside and this causes the temperatures to equalize. We also can see a relative humidity gradient inside the chamber influenced by the goods stored.

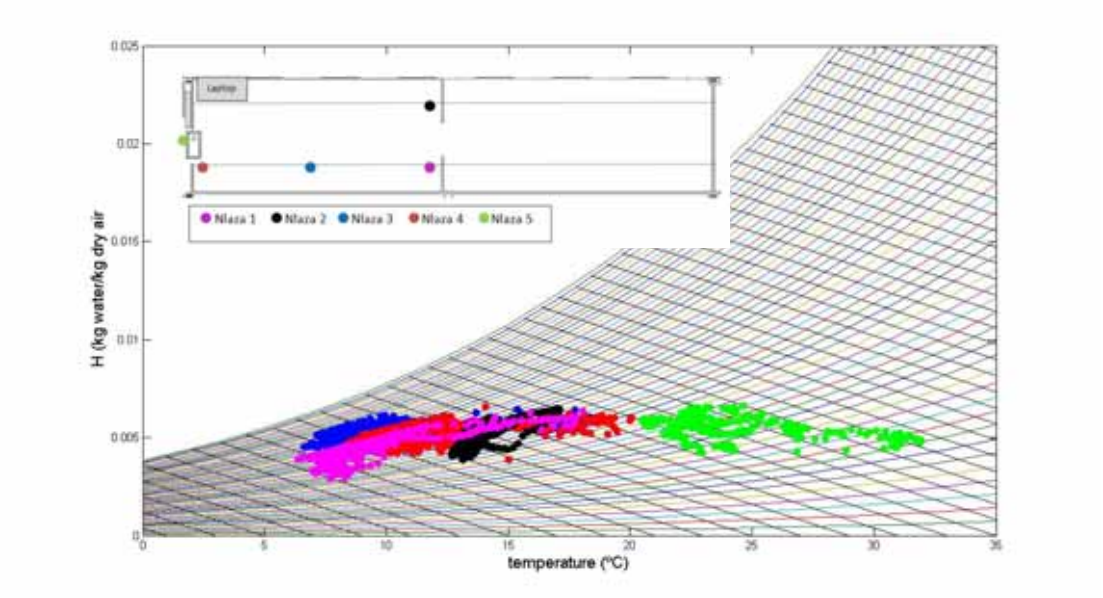

Figure 13. Psychrometric chart for cold chamber number 40 data.

As we see in **Figure 13**, the closer to the door the sensors are, higher temperature is reached by them. On the other hand, Nlaza 2 mote (black points) is always warmer than others inside the chamber because much of the time there is an operator working in that area.

There is a correlation between energy consumption billed by the warehouse holder and the calculated air enthalpy (see **Figure 14**). Air enthalpy changes continuously due to temperature variations inside the cold chamber. Enthalpy peaks usually correspond to door opening and thus there are large increases in energy consumption as well. The Energy Consumption data are recorded every hour and the enthalpy of the air every three minutes, so a Power Consumption peak can correspond to multiple jumps of the air enthalpy. Refrigeration system also starts running to compensate for the thermal inertia of the cold chamber. We can address this fact **Figure 14**. Sometimes, mechanical failures on the inlet valve of cold glycol cause errors in the energy billing. This can be diagnosed by comparison between the energy consumption and the variation of the air enthalpy (see **Figure 14**).

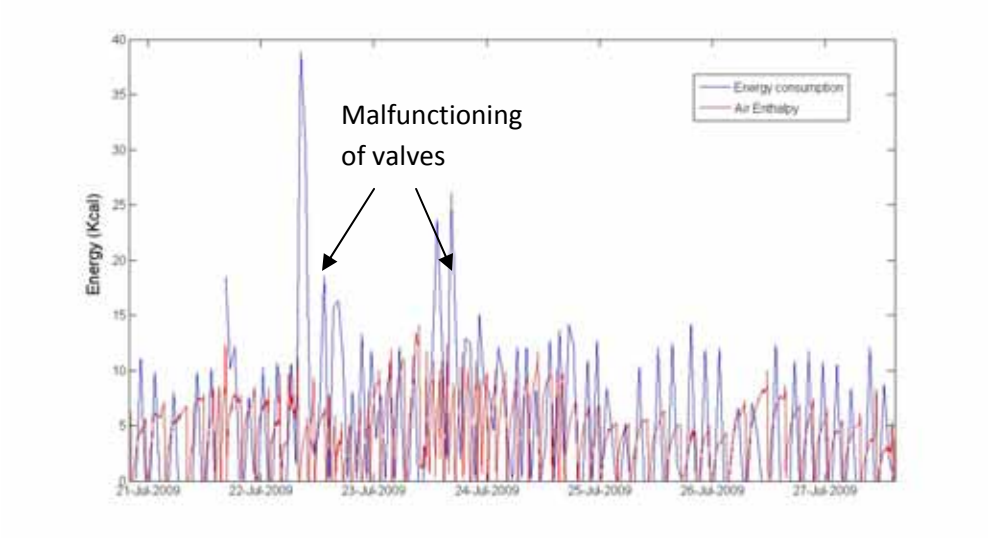

Figure 14. Air enthalpy and power consumption in cold chamber number 29.

When there is correlation between power consumption and air enthalpy, the subtraction between them will fluctuate around a mean value. We show this behavior in **Figure 14**. Values outside the control limits can be assigned to malfunctioning of the valves and thus billing errors occur.

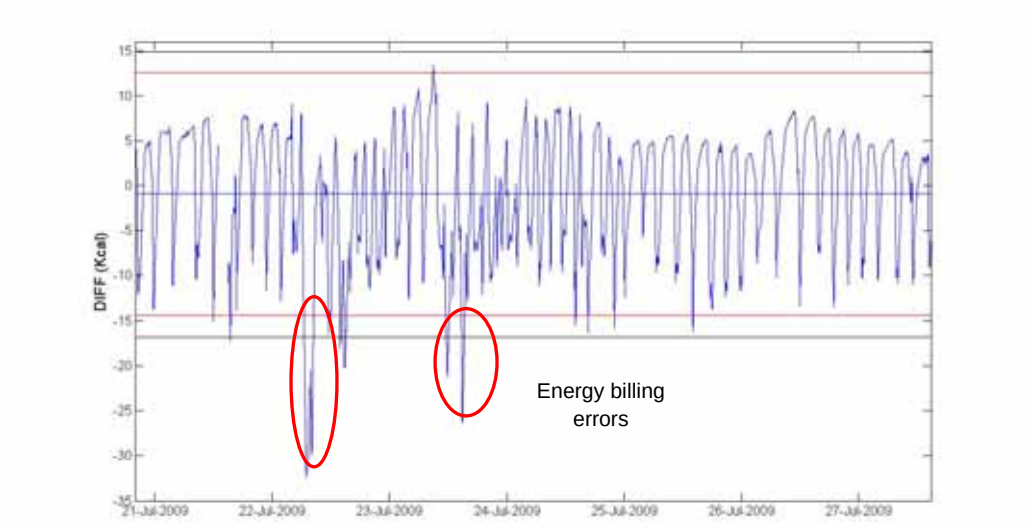

Figure 15. Difference between the Air Enthalpy and the Power Consumption in chamber 29; two faults are diagnosed.

For cold chamber 29, the difference between Air Enthalpy and Power Consumption is -0.9Kcal, and de standard deviation is ±6.9Kcal. With those data we calculate the range where the 95 or 98 per cent of normal data are found. Out of these limits we can guess that errors are occurring in the energy billing (see **Table 4**).

Table 4. Limits for detecting malfunctioning in cooling system and for defining energy billing errors.

	95% (t=1.96)	98% (t=2.32)
Upper limit	12.6Kcal	15.0Kcal
Lower limit	-14.4Kcal	-16.8Kcal

Main achievements: the use of temperature and relative humidity together with psychrometric models allow defining smart capabilities for sensors. Difference in absolute humidity along chambers, air flow across the doors and energy balance are also smart functions that can easily be incorporated on smart sensors. Smart capabilities allow addressing faults and malfunctioning in the cooling systems. Therefore smart capabilities become system diagnosis at very low cost and high frequency rate. In this framework, wireless sensor motes proved to be flexible and useful for a user-friendly data monitoring system.

SMART SENSORS FOR SOLAR WOOD DRYING

As final case study, we propose the smart supervision of solar dryers. The starting point for this case study states that wood drying is the highest energy consumer with about 70 percent of the total energy used in the manufacturing of most wood products. Since the 1960s, several types of solar kiln for timber drying have been studied and improved on, due to some advantages of the solar kilns, as lower or no operating cost since no fuel is needed for air heating. On the other hand the main disadvantage is its dependence on the alternating day/night, seasonal rhythms and weather conditions, resulting in less controllability by the operator, and less predictable outcomes. The definition, implementation and integration of intelligent sensors in solar dryers as simulation and optimization tools, which is faced in this paragraph has been submitted to Solar Energy for publication (Correa-Hernando et al., 2010).

Instrumented dryer Low cost sensors are most suitable for the supervision and control of solar dryers, and can be easily upgraded by including smart capabilities. As stated before, the Sensirion SHT is a single chip relative humidity and temperature multisensor module that delivers a calibrated digital output useful to characterize the drying air. On the other hand, thermocouples type T (copper-constantan) stuck on wood surface measure wood temperature.

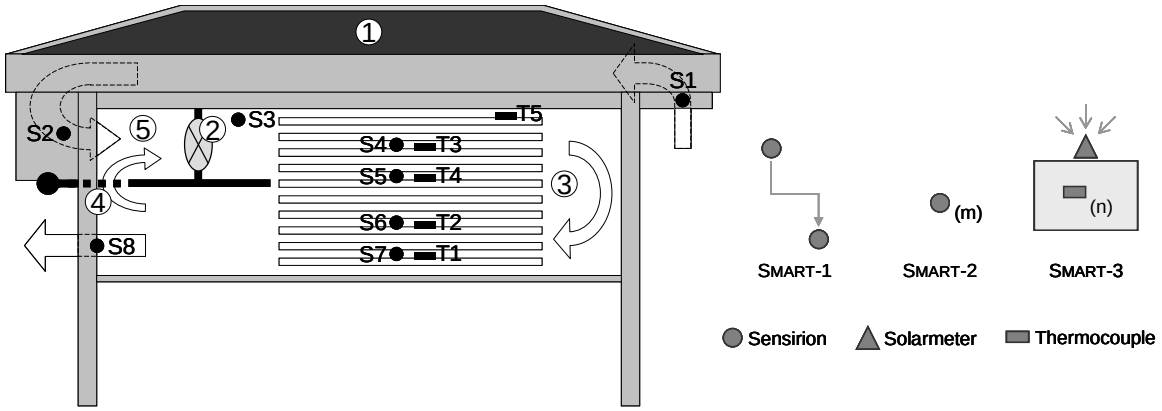

Figure 16. Left: scheme of the solar dryer, solar collector (1), fan (2), chamber for drying (3), gate for recirculation of air (4), and plenum chamber (5). The arrows indicate the airflow. Also, the location of the eight Sensirion S1-S8 (•) and the five thermocouples T1-T5 (▪) is indicated. Right: schematic representation of the proposed Smart sensors, type and (number) of sensors required is presented

The ubiquitous distribution of sensors in the dryer allows a multidistributed supervision of drying kinetics inside the dryer kiln. In this sense, a net of eight Sensirion sensors and five thermocouples were located at different positions in an experimental solar dryer. The dryer has a capacity of 0.3 m^3, is equipped with a solar collector of 2 m^2, a 12 V DC fan, a chamber for drying, various metallic trays where samples of pine (*Pinus sp*.) wood were placed, and a gate that controls the recirculation of air and a plenum chamber (see **Figure 16**). The sensors were connected by wire to a board with a PIC (Peripheral Interface Controller) microcontroller. In the PIC the signals are multiplexed and then sent to a computer.

Proposed mathematical models

Psychrometric model, already been cited in previous case studies. Absolute humidity H (water mass over dry air mass), wet bulb humidity H_w (water mass over dry air mass), wet bulb temperature τ_w, specific volume V_s (air volume over dry air mass) and specific enthalpy h (enthalpy over dry air mass), characterized the air at each Sensirion localization.

Smart-1. Two Sensirion sensors were considered: one located at the drying chamber inlet (after mixing with the recirculation air, S3 in **Figure 16**), and the other one at the dryer outlet (S8 in **Figure 16**). The estimation of the extracted water from the timber during each working day from the absolute humidity of the air is the base of the Smart-1. The difference of absolute humidity of the air at the outlet H_{out} and at the inlet H_{in} of the drying chamber is considered to be the extracted water H_{ext}. At each time t the mass of extracted water per mass unit of dry air were computed according to

$$H_{ext} = H_{out} - H_{in}. \qquad \text{Eq. 6}$$

Considering the air density ρ as the inverse of the specific volume, and the flux of ventilator Q, the rate of wood water extracted is computed as

$$\frac{dH_{\text{ext}}}{dt} = -\rho Q H_{\text{ext}} \,. \qquad \text{Eq. 7}$$

The integration of the previous expression allows us to estimate the loss water of the wood for each working day. The accumulated water extracted along the complete drying cycle was compared with the reference measurements, base on the gravimetric determination (see **Figure 17**).

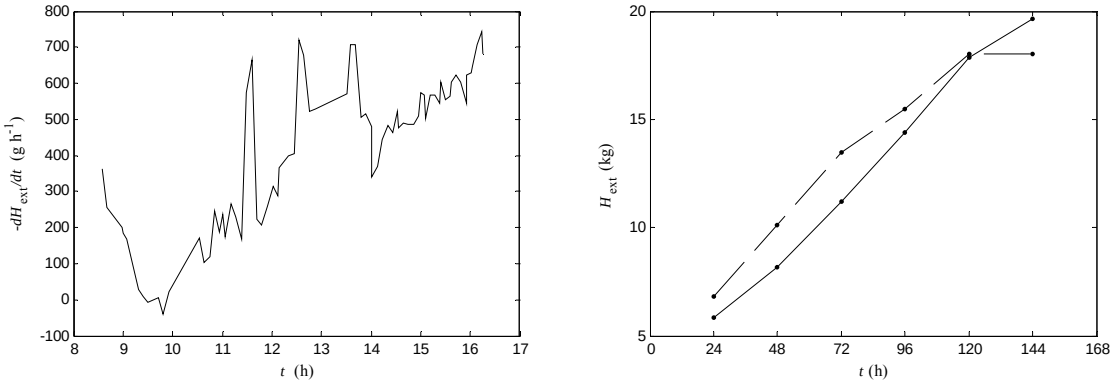

Figure 17. Left: rate of wood water extracted $-dH_{ext}/dt$ along one drying day. Right: accumulated wood water extracted along a complete drying cycle H_{ext} estimated with Smart-1 (solid line) and gravimetric experimental measurement (dashed line)

Smart-2. It is possible to define a smart sensor based on the temperature and relative humidity of the air inside the kiln, measured for the net of eight Sensirion sensors. This smart sensor will allow determining the drying rate and the timber moisture distribution into the dryer.

The drying rate expressed as $-dM/dt$, where M is the oven dry wood moisture (water mass over oven dry wood mass), allows identifying two different kinetics: one with a constant drying rate, for surface moisture M_s above the fiber saturation point M_{FSP}, and a second one for M_s below the M_{FSP} value, characterized for a decreasing drying rate.

For $M_s \geq M_{FSP}$, the drying process depends, as external parameters, only on the temperature and the absolute humidity of the drying air. Geankoplis (Geankoplis, 1983) proposed the heat and mass transfer balances that allow defining the constant drying rate as Eq. 8

$$-\frac{dM}{dt}=\frac{A\sigma(\tau-\tau_w)}{m_{dry}q_{vap}}, \qquad \text{Eq. 8}$$

where the difference between the dry air τ and wet bulb τ_w temperatures acts as the impulsive force of this process. *A* is the drying area, m_{dry} is the dry mass of the timber, and q_{vap} is the latent heat of vaporization of wood water per mass unit at the temperature τ_w. Magnitude σ is the convection heat transfer coefficient of the air, again defined by Geankoplis as $\sigma = kG^{\zeta}$, where *G* is the mass flux density of the air, calculated as $G = Q(1+H)/SV_s$, being *Q* the flux of the ventilator, *H* absolute humidity, *S* the cross section for drying air circulation, and V_s the specific volume.

Table 5. Parameters and input arguments for the equations used in the model Smart-2 for wood drying. (*) Values reported for softwoods as the pine one (Smith and Langrish, 2008).

A	7 m^2	*M0*	0.6
mdry	60 kg	*L*	0.0125 m
Q	0.11 $m^3 s^{-1}$	*D_0	1.30 10-4 m2 s^{-1}
S	0.004 m^2	*E_a	1776.297 kJ kg^{-1}
k	14.278	*R*	0.4615 kJ kg^{-1} K^{-1}
ξ	0.8		

For $M_s \le M_{FSP}$, diffusion is the mechanism that governs a decreasing drying rate at this stage (Khater et al., 2004). Eq. 9

$$-\frac{dM}{dt}=\frac{2M_0}{L^2}\left(t\frac{dD}{dt}+D\right)\exp\left(-\left(\frac{\pi}{2L}\right)^2 Dt\right), \qquad \text{Eq. 9}$$

enables the drying rate calculation at low moisture content. This corresponds to the derivative with respect to time of the first term of the series of Fick's law solution for an infinite plate (one-dimensional problem, (Crank, 1979) (Luikov, 1968)) and for a moisture content at timber surface taken negligible because it assumed a dry hot air surrounding that avoid to stay water at timber surface. *M* and M_0 are the averaged wood moisture content at any time *t* and *t = 0* respectively. *L* is the half thickness of food and *D* represents the temperature dependent diffusion coefficient defined by the Arrhenius equation Eq. 10)

$$D = D_0 \exp\left(-\frac{E_a}{RT}\right). \qquad \text{Eq. 10}$$

Where D_0 is the reference diffusion coefficient, E_a is the activation energy, R is the universal gas constant and T is the absolute temperature of wood taking into account that for this second drying period it has been consider negligible the difference between T and τ.

The Smart-2 model is defined for the combined resolution of Eq. 8, Eq. 9 and **Table 5** that allow recalculating in real time a changeable drying rate (see **Figure 18**) according with the temperature and absolute humidity of the air measured with the Sensirion in different positions inside the kiln. The integrated form of these equations provides the evolution of wood moisture content for the constant drying rate and the decreasing drying rate kinetics (see **Figure 18**).

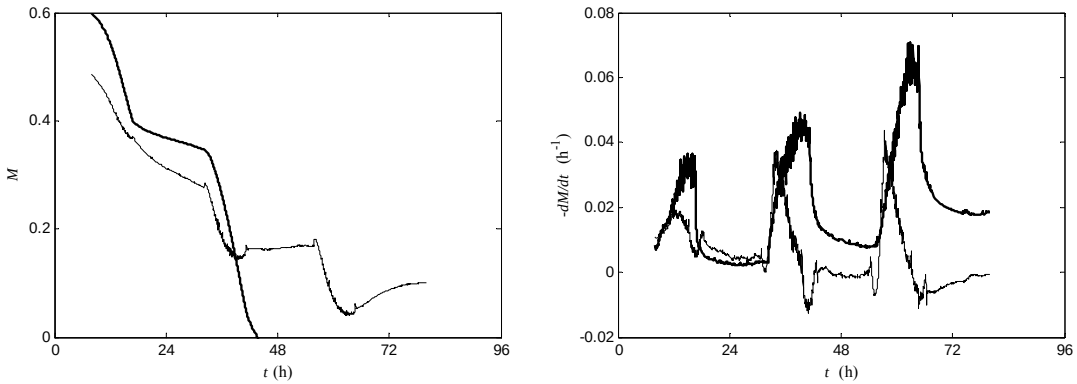

Figure 18. Left: evolution of oven dry wood moisture M along one drying cycle for $M_s \geq M_{FSP}$ (thick line) and for $M_s \leq M_{FSP}$ (thin line). Right: evolution of drying rate for a constant drying rate (thick line) and for a decreasing drying rate (thin line). τ and H data corresponding to Sensirion S3.

The possibility of acquiring temporal profiles of temperature and relative humidity of the air inside the kiln with our instrumented solar dryer is the basis for simulation. **Figure 19** shows the result of a simulation carried out taking into account ten different product loads (m_{dry} from 48 to 135 kg) and evaporating areas (A from 7 to 2 m^2) inside the kiln, obtained as a function of the thickness of the wood plank (L from 0.01 to 0.05 m) using for the rest of parameters and input arguments data from **Table 5** at the Smart-2 model compilation.

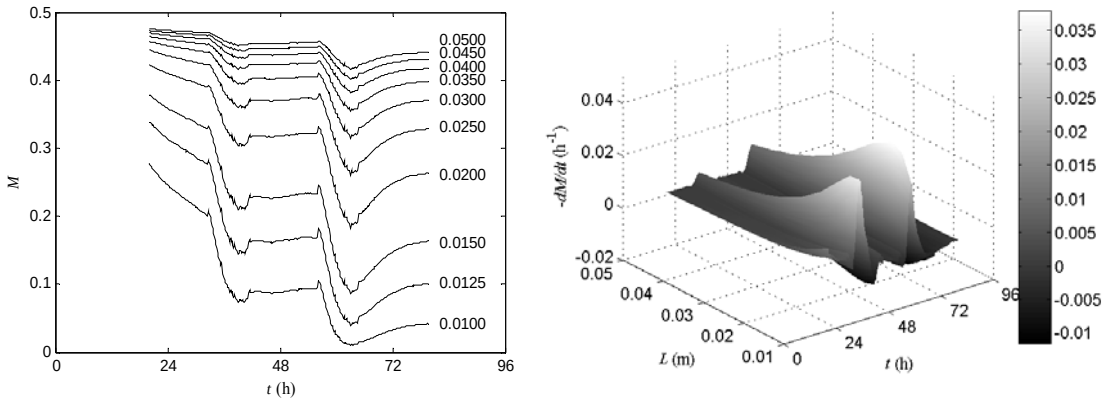

Figure 19. Left: simulation of evolution of oven dry wood moisture M along one drying cycle Ms ≤ MFSP for different thickness of the wood plank. The thickness has been indicated in meters. Right: simulation of evolution of drying rate for different thickness of the wood plank L. The τ and H data correspond to Sensirion S3.

Smart-3. We can define a smart sensor based on the temperature distribution data of the wood into the dryer obtained from thermocouples and solar radiation data. This smart sensor will provide us the wood moisture distribution into the dryer and the energy efficiency of the drying process.

For each daily cycle we have essentially (see **Figure 20** left), neglected short time oscillations, a minimum temperature (T_{min}) corresponding to night cooling, and a maximum temperature (T_{max}) due to the solar midday. T_{min} is approximately the same for every cycle. However, although the solar radiation is similar every day T_{max} increases for each cycle. This behavior can be understood by means of a simple energy balance and considering the thermodynamics of the dry process. We can consider that the solar radiation energy E_{rad} is used to heat the wood (E_{heat}) and evaporate the water (E_{vap}), namely where E_{loss} represents the energy losses

$$E_{\text{rad}} = E_{\text{heat}} + E_{\text{vap}} + E_{\text{loss}} \,. \qquad \text{Eq. 11}$$

Since the wood moisture decreases for successive cycles, and the wood heat capacity (C_p) also decreases when the wood moisture decreases, the same energy will produce a greater temperature for successive cycles. Moreover, due to the wood moisture decreasing, the amount of evaporated water will be less for successive cycles, then the water vaporization energy will be less too, and a greater amount of energy will be used to heat the wood.

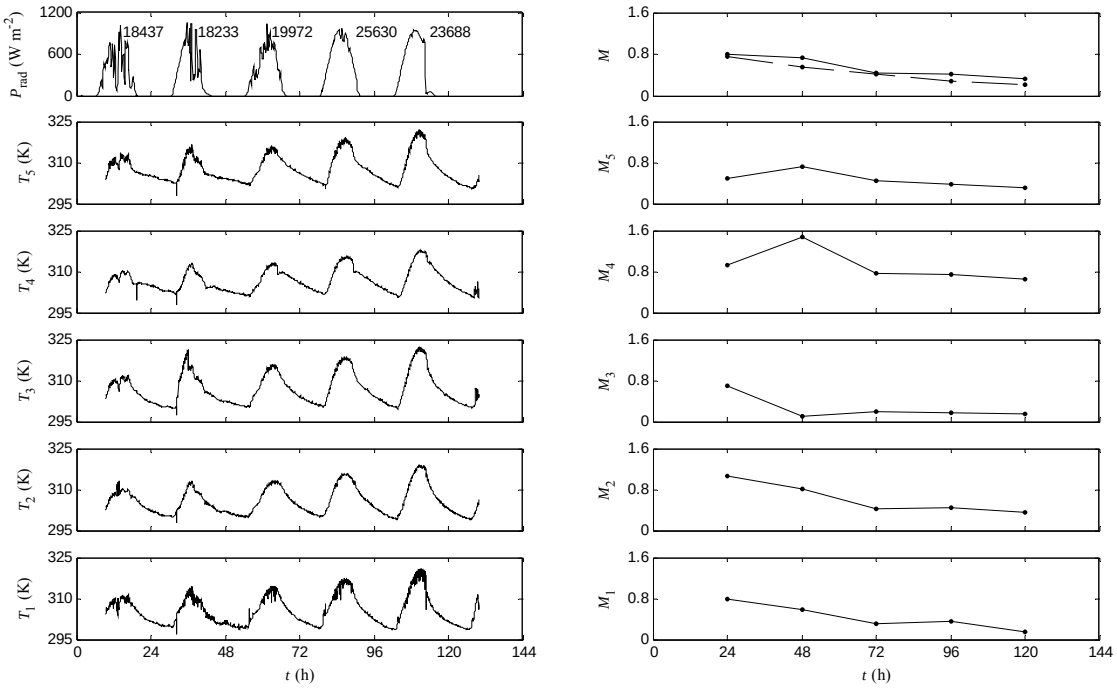

Figure 20. Left: (top panel) density of power (kJ m^{-2}) of the solar radiation P_{rad} along five solar cycles. (All other panels) Temperature data of the five thermocouples T_1-T_5, along the same five solar cycle. Right: (top panel) time evolution of the average of the wood moisture calculated for each thermocouple position (solid line) and experimental wood moisture (dashed line). (All other panels) Time evolution of the wood moisture estimated for each thermocouple position M_1-M_5 corresponding to the temperature data T_1-T_5 in the left figure

The wood C_p can be expressed as a function of the oven dry wood moisture M and wood temperature T (see Wood Handbook (1999), Ch. 3). Considering the definition of the heat capacity, that is $C_p = (\partial q/\partial T)_p$, the integration of wood C_p equation between T_{min} and T_{max} for every daily cycle, gives an expression for the energy (per mass unit) $q_{heat} = E_{heat}/m_{heat}$ needed for the heating. Reorganizing this expression we can obtain a polynomial in the variable M or in the variable T. The root of each one of these polynomials with physical meaning will give us the wood moisture and T_{max}.

On the other hand, we have the energy used to evaporate the water. This energy corresponds to the enthalpy of vaporization plus, if no fiber saturation, the energy of the wood–water bond (q_{bond}). We can obtain the enthalpy of vaporization for a temperature T as the difference between the enthalpy of saturated vapor $h_v(T)$ and saturated liquid $h_l(T)$ (see data for water/steam refrigerant R-718 in (ASHRAE, 2005)). So that, we can obtain the energy of vaporization (per mass unit) $q_{vap} = E_{vap}/m_{vap}$ as an average of the h_v in the interval of

temperatures corresponding to the T_{min} and T_{max} of each daily cycle, plus a term corresponding to q_{bond} (see Eq. 13 in Briggs, 1994).

$$q_{vap} = \frac{1}{T_{max} - T_{min}} \int_{T_{min}}^{T_{max}} dT \left[h_v(T) - h_l(T) \right] + q_{bond} \ , \qquad \text{Eq. 12}$$

where

$$q_{bond} = \begin{cases} 316.32 \text{ kJ kg}^{-1} \text{ if } M \le M_{FSP} \\ 0 \qquad \text{kJ kg}^{-1} \text{ if } M > M_{FSP} \end{cases} . \qquad \text{Eq. 13}$$

Finally, we need the solar radiation data (density of power $P_{rad}(t)$) provided by a meteorological station (see **Figure 20**) to calculate the solar energy received by the dryer along each daily cycle. Namely,

$$E_{rad} = S \int_{t_1}^{t_2} dt \ P_{rad}(t) \ , \qquad \text{Eq. 14}$$

where S is the surface of the dryer solar panel, and t_1, t_2 is the time interval corresponding to a solar cycle.

The information supplied by this model Smart-3, together with that of models Smart-1 and Smart-2, allows us to calculate the total energy efficiency of the dryer $\xi_{total} = (E_{heat}+E_{vap})/E_{rad}$, and the vaporization energy efficiency $\xi_{vap} = E_{vap}/E_{rad}$ as can be seen in Figure 21. Moreover, it is possible to estimate the moisture distribution into the dryer associated to the position of each thermocouple (see **Figure 20** right). For this purpose, the averaged T_{min} and T_{max} are used to obtain the value of the heating energy, then this value is used in order to estimate the moisture for every thermocouple.

Main achievements: Three Smart mathematical models, implemented in *ad hoc* Matlab routines time depending, are proposed in this work. The simplest smart sensor, Smart-1, using only two Sensirion sensors, allows to estimate the accumulated wood water extracted along a complete drying cycle with a correlation coefficient of 0.97 with the gravimetric experimental measurement (see **Figure 17**).

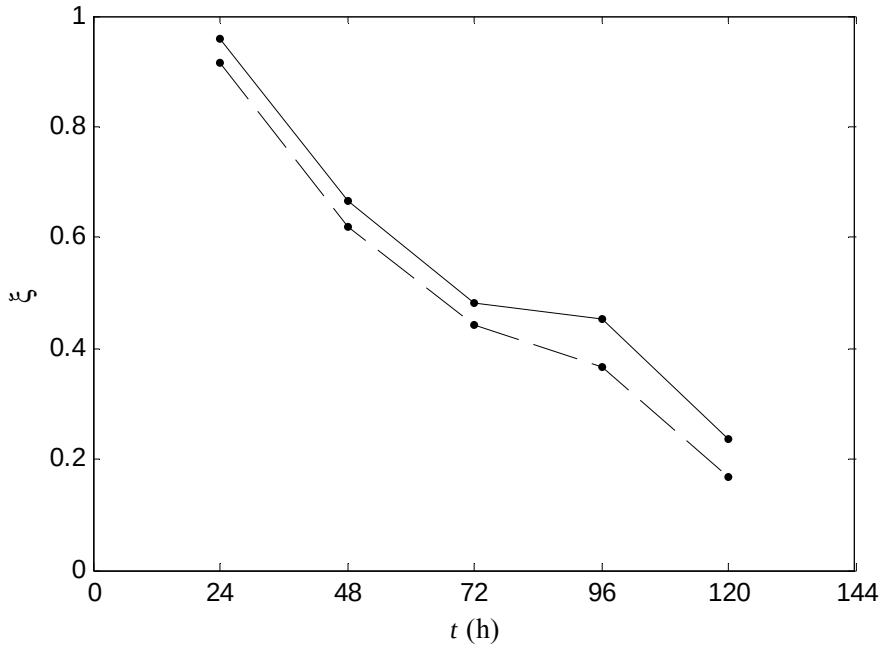

Figure 21. Evolution of the total energy efficiency ξ_{total} (solid line) and vaporization energy efficiency ξ_{vap} (dashed line) of the dryer throughout the drying process.

In the Smart-2 model the point where the two drying kinetics (constant and decreasing drying rates) coincide, it is consider as the critical point which establishes the end of the constant drying rate period and the beginning of the decreasing drying rate one (Fito et al., 2001). **Figure 18** (right) shows that in the drying cycle studied this occur after an initial period of constant drying rate of 18 hours. In **Figure 18** (left) averaged wood M values between 0.4-0.38 corresponds at this stage with the moment where $M_s = M_{FSP.}$ The drying period from $M_s = M_{FSP}$ to reach the M_{FSP} at wood center (typically at M = 0.3) it is consider as a transition drying period, from 18 to 30-36 drying hours in this work (t values for M = 0.3). The end of this transition period marks the beginning of the diffusion phenomenon (Fernández-Golfín J. I. and Conde, 2007). The effect of product load inside the kiln is also clear in simulation shown in **Figure 19**. For increasing L values, higher M values are estimated for each time due to a slower drying rate. Considering M = 0.3 as the beginning point for a correct estimation of M and $-dM/dt$ during the decreasing drying rate period, the wood corresponding to the four highest thickness do not reach this value not even after three days of drying. The identification of these drying periods not only allows the correct estimation of M and $-dM/dt$ in function of the drying kinetics but also as simulation tool will allow optimizing dryer design and dryer regulations and control for each period and weather conditions.

Moreover, as we can see in Figure 21, the model Smart-3 indicates a decreasing efficiency along the drying process. This fact is due to the known effect of efficiency fall as the moisture decreases (Fernández-Golfín et al., 2007). However, we can observe a recuperation of the efficiency between the third and fourth drying cycles (72 to 96 h). This recuperation seems to correspond to the inhomogeneous drying of the wood (see **Figure 20** right) addressing specially

for the moisture increases of wood located in the inner center of the dryer corresponding to the position of the thermocouples T4. Further experiments are mandatory to design a control strategy (by means of the fan velocity and the recirculation gate) in order to improve the energy efficiency. Undoubtedly, a more homogeneous drying will improve the energy efficiency and also the quality of the wood.

CONCLUSIONS

The use of Smart Sensors response as an input for Smart Control is sketched in the document, and methods and tools for Smart Controls described.

Several case studies have been selected: the Smart Concept for animal welfare, Smart Supervision of fruit storage and transport, Smart Sensors for solar wood drying, which have been very recently developed and that are in their way to become scientific publications in the very near future.

A main conclusion of this work is that it is feasible and cheap to turn a standard integrated sensor into a smart one, in a process that we shall call sensor education.

Further development will include spatially distributed models within the sensor board as to estimate the quality evolution inside 3D models foods.

Complex multisensory systems with ubiquitous measurements will be used in the near future as information source under Smart Control Strategies: optimal experimental design, and predictive control.

The aforementioned knowledge can be easily exported to other fields such as Smart Agricultural Machines, where plant-level systems and soft machine-plant interaction is required.

REFERENCES

Arguenon, V., A. Bergues-Lagarde, et al. 2006. Multi-agent based prototyping of agriculture robots. 2006 International Symposium on Collaborative Technologies and Systems, Proceedings: 282-288.

Aguilera, J.M. 2000. Microstructure and food product engineering. Food Technol. 54(11): 56-65

Aguilera, J.M. 2004 Why food microstructure? J. Food Eng.. 67: 3-11

Alonso, A.A.., Kevrekidis, Y.G., Banga, J.R., Frouzakis, C.E. 2004. Optimal sensor location and reduced order observer design for distributed process systems. Comp. & Chem. Eng. 28, 27

ASABE_Standards. 2006. Psychrometric data ASABE D271.2 APR1979, R2005. St.Joseph, MI.

ASHRAE. 2005. Handbook-Fundamentals (SI) American Society of Heating, Refrigeration, and Air-Conditioning Engineers, Atlanta.

Balsa-Canto E, Rodriguez-Fernandez M, Banga JR. 2007. Optimal design of dynamic experiments for improved estimation of kinetic parameters of thermal degradation. J. Food Eng 82 (2): 178-188

Briggs D. 1994. Forest products measurements and conversion factors University of Washington, Institute of Forest Resources, Seattle.

Bruin S, Jongen ThRG. 2003. Food Process Engineering: the last 25 years and challenges ahead. Comprehensive Reviews in Food Science and Food Safety 2:42-81.

Cook, B. W., S. Lanzisera, et al. 2006. SoC issues for RF smart dust. Proceedings of the Ieee 94(6): 1177-1196.Crank J. (1979) The Mathematics of Diffusion Clarendon Press.

Correa-Hernando, E; Arranz, FJ; Diezma, B; Juliá, E ; Robla, JI; Ruiz-García, L; García-Hierro, J; Barreiro, P. 2010. Development of smart sensors for the supervision of a wood solar dryer. Part I: The models. Solar Energy (submitted)

Datta AK. 1998. Computer-aided engineering in food process and product design. Food Technology 52(10):44-52.

De Smedt, V; Barreiro, P; Verlinden, B.E.; Veraverbeke, E.A.; De Baerdemaeker, J; Nicolai, B.M. 2002. A mathematical model for the development of mealiness in apples. Postharvest Biology and Technology 25(2002) 273-291

Durfee, W. K. 1995. Designing smart machines.- teaching mechatronics to mechanical engineers through a project based, creative design course. Mechatronics 5(7): 775-785.

Fernández-Golfín J. I., Conde M. 2007. Manual técnico de secado de maderas Asociación de Investigación Técnica de las Industrias de la Madera y el Corcho (AITIM)

Fito P., Andrés A.M., Barat J.M., Albors A.M. 2001. Introducción al secado de alimentos por aire caliente Departamento de Tecnología de los Alimentos, Universidad Politécnica de Valencia., Valencia.

Garcia MR, Vilas C, Banga JR, Alonso AA. 2007. Optimal field reconstruction of distributed process systems from partial measurements. Ind. & Eng. Chem. Res. 46(2): 530-539

Garcia Hierro, J; Barreiro, P; Ruiz-Garcia, L; Robla, JI. 2010. Development of smart sensing device for ubiquitous supervision of the cold chain: application to perishable commodities. International Conference on Agricultural Engineering AgEng. Clermont Ferrand (France) 6.8 September

Geankoplis C.J. 1983. Drying of process materials, transport processes and unit operations Allyin and Bacon, Boston.

Isermann, R. 2006. Sensors. CIGR handbook of Agricultural Engineers Chapter 2. ISBN 1892769549.

Jurianse, A.C. 1999. Changing pace in food science and technology: Examples from dairy science show how descriptive knowledge can be transferred into predictive knowledge. Trends in Food Sci. & Technol. 10(9): 303-306

Khater H.A., Helwa N.H., Enayet M.M., Hashish M.I. 2004. Optimization of Solar Kiln for Drying Wood. Drying Technology 22:677-701.

Luikov A.V. 1968. Analytical Heat Diffusion Theory University of Illinois, Department of Energy Engineering.

Qin SJ, Badgwell TA. 2003. A survey of industrial model predictive control technology. Control Eng. Practice 11:733-764.

Rodriguez-Fernandez M, Balsa-Canto E, Egea JA, Banga JR. 2007. Identifiability and robust parameter estimation in food process modelling: Application to a drying model. J. Food Eng 83 (3): 374-383

Rodriguez-Bermejo, J., P. Barreiro, et al. 2007. Thermal study of a transport container. Journal of Food Engineering 80(2): 517-527.

Ruiz-Garcia, L., P. Barreiro, et al. 2008. Performance of ZigBee-based wireless sensor nodes for real-time monitoring of fruit logistics. Journal of Food Engineering 87(3): 405-415.

Ruiz-Garcia, L., P. Barreiro, et al. 2010. Testing ZigBee Motes for Monitoring Refrigerated Vegetable Transportation under Real Conditions. Sensors 10(5): 4968-4982.

Ruiz-Garcia, L., P. Barreiro, et al. 2007. Review. Monitoring the intermodal, refrigerated transport of fruit using sensor networks. Spanish Journal of Agricultural Research 5(2): 142-156.

Ruiz-Garcia, L., L. Lunadei, et al. 2009. A Review of Wireless Sensor Technologies and Applications in Agriculture and Food Industry: State of the Art and Current Trends. Sensors 9(6): 4728-4750.

Ruiz-Garcia, L., G. Steinberger, et al. 2010. A model and prototype implementation for tracking and tracing agricultural batch products along the food chain. Food Control 21(2): 112-121.

Sasha, V.I., T.A. Haley, R.K. Singh. 2001. A survey of automation practices in the food industry. Food Control 12:285-296.

Saraiva, AM; Hirakawa, AR; Cugnasca, CE. 2006. Topics on software evolution. CIGR handbook of Agricultural Engineers Chapter 3. ISBN 1892769549.

Smith S.A., Langrish T.A.G. 2008. Multicomponent Solid Modeling of Continuous and Intermittent Drying of Pinus radiata Sapwood Below the Fiber Saturation Point. Drying Technology 26:844 -854.

Tomizuka, M. 2002. Mechatronics: from the 20th to 21st century. Control Engineering Practice 10(8): 877-886.

Van Wylick .2009. Smart Products. http://www.techiteasy.org/2009/01/07/smart-products/

Villarroel, M; Barreiro, P; Kettlewell, P; Farish, M; Mitchell, M. Relative changes in air temperature and enthalpy as non-invasive welfare indicators during animal transport. Biosystems Engineering (submitted)

Wise, K. D. 2007. Integrated sensors, MEMS, and microsystems: Reflections on a fantastic voyage. Sensors and Actuators a-Physical 136(1): 39-50.